Indonesian Journal of Electrical Engineering and Computer Science
Vol. 43, No. 1, July 2026, pp. 103~113
ISSN: 2502-4752, DOI: 10.11591/ijeecs.v43.i1.pp103-113

Pulmonary nodule in CT image quantification by using pulmonary nodules magnitude ratio

Asharani Ramadas[1,2], Chidananda Murthy Melekote Vinayakamurthy[3]
[1]Department of Electronics and Communication Engineering, Sri Siddhartha Academy of Higher Education, Karnataka, India
[2]M. S. Ramiah College of Arts, Science and Commerce-Autonomous, Karnataka, India
[3]Sri Siddhartha Institute of Technology, Sri Siddhartha Academy of Higher Education, Karnataka, India

Article Info

Article history:

Received Mar 16, 2026
Revised Jun 14, 2026
Accepted Jun 27, 2026

Keywords:

CT image
Pulmonary nodule
Pulmonary nodule magnitude ratio
Segmentation
Synthetic nodule

ABSTRACT

The growth rate of the Pulmonary nodule increases the doubling time of the Pulmonary nodule, which is a significant indicator of malignancy. The mean diameter measurement of the Pulmonary nodule contributes to the assessment of lung cancer based on the doubling time. Small nodule size, partial volume effect, irregular shape, juxtapleural, and juxtavascular nodules are difficult to measure. This work addresses these measurement challenges using an image processing pipeline consisting of image segmentation and quantification. The computed tomography (CT) image preprocessing, segmentation, edge detection, and nodule measurement framework is proposed to extract the nodules from the CT image and then quantify them by measuring their mean diameter. A novel pulmonary nodules magnitude ratio (PNMR) is proposed to establish the sattastical relationship between the nodule and corresponding parenchyma size. The PNMR is evaluated against the synthetic nodules that express the nodule growth rate. This work contributes automatic nodule detection, semiautomatic nodule measurement, and PNMR evaluation for more reliable detection and quantification of Pulmonary nodules.

Corresponding Author:

Asharani Ramadas
Department of Electronics and Communication Engineering, Sri Siddhartha Academy of Higher Education
Maralur, Tumkur 572105, Karnataka, India
Email: asha.srp@gmail.com

1. INTRODUCTION

Lung cancer is the most common cancer with a high mortality rate. Accurate nodule assessment, growth rate monitoring, rapid diagnosis, and timely treatment increase the survival rate. Evaluation of tumor growth rate as an independent diagnostic marker, prediction of tumor growth rate, and early detection of malignant nodules are the future research directions for lung cancer screening. Careful monitoring of nodule growth and growth rate is a critical factor in lung cancer screening [1]. Nodule growth rate is a potential indicator of malignancy. Growth rate contributes to early identification of lung cancer, clinical intervention, and necessary follow-up for effective lung cancer management [2]. Manual diameter measurement is used when the volume measurement is unreliable for an accurate assessment of pulmonary nodule growth, and the same measurement is used in subsequent lung CT images. The manual measurement is necessary for attached nodules, cystic nodules, and solid components of subsolid nodules. The diameter taken is the average of the larger axial, perpendicular, and craniocaudal diameters. If the volumetric assessment fails, the growth rate is defined using the increase in diameter per year or the longest follow-up intervals [3]. AI-assisted LDCT screening consisting of nodule detection, segmentation, and measurement improves the consistency of nodule evaluation and supports an effective nodule management system [4]. An AI-aided pulmonary nodule

diagnosis system improves radiologist efficiency over the period of implementation [5]. Nodule detection, early cancer detection, consistent forecasting, and reducing the workload of radiologists are the potential benefits of AI integration in systems for diagnosing lung cancer, even though it requires human intervention due to the chance factor of false positives [6]. GPT-4o can perform several key tasks of a radiologist as routine work during the assessment of pulmonary nodules. It can analyze the longitudinal CT scans and show strong predictions for malignancy and nodule assessment; further real-world validation is required before clinical deployment [7]. The CT slice thickness of a CT image is an important factor that affects the nodule's radiomics measurement in lung cancer screening [8]. A commercial CAD system for pulmonary nodule detection performs slightly worse than expert radiologists, but it can assist with nodule detection, automatic measurement, and characterization of nodules. Further improvement is required while handling nodule texture to distinguish solid, partially solid, and ground glassy nodules [9].

DL-CAD systems effectively detect the pulmonary nodules but still struggle with accurate nodule characterization, volumetric assessment, and characterization, especially for partially solid nodules [10]. Volume-based nodule assessment is more accurate than the diameter-based assessment; if it is unsuccessful, then diameter assessment is used in lung cancer screening [11]. Mean diameter assessment for nodule evaluation is an important method supplemented by the volumetric assessment of nodules and AI tools in lung cancer screening. It is a fallback method where the AI and volumetric software fail to assess the pulmonary nodules. This study proposes an image processing-based framework for pulmonary nodule assessment. The proposed method aims to automatically segment nodules, semiautomatically measure nodules, and establish the PNM for nodule assessment. The proposed model is evaluated against the synthetic nodules. The major contribution of this work is stated:

- Pulmonary nodule segmentation using CT images.
- Synthetic nodule generation.
- Pulmonary nodule means diameter measurement.
- Pulmonary nodule magnitude ratio to establish a relationship between nodules and lung parenchyma.

This paper is structured as follows: Section 2 covers the materials and methods; section 3 comprises results and discussion. Finally, section 4 comprehends the conclusion.

2. MATERIALS AND METHOD

2.1. Dataset

The lung CT images are obtained from the LIDC-IDRI dataset from the Kaggle website (https://www.kaggle.com/datasets/jokerak/lidcidri) [12]. It is a publicly available open access dataset for research and CAD development. The data set is organized into several folders containing original CT images, corresponding nodule masks, regions of interest (ROIs) for nodules, boundary-enhanced ROI images, mask ROIs, and XML annotation files. In this study we make use of lung CT images and corresponding nodule mask folders. There are 7,521 original CT images in the image folder and 7,521 segmented nodule masks in the mask folders. Few diverse pathological structures and intensity variations in image samples are considered for simulation work.

2.2. Proposed method

The methodology of the nodule detection and measurement is demonstrated in Figure 1. The proposed method reads CT images from the LIDC-IDRI dataset of resolution 512×512. The CT images have low contrast between the lung nodules and surrounding lung tissue; small nodules often exhibit the same contrast as lung tissue. Hence, the input image is contrast-enhanced, and pixel intensities ranging from 0.02 to 0.6 are stretched to the grayscale range [0, 1]. Gamma corrections are employed for nonlinear contrast enhancement and preserve the significant image features that help distinguish between nodules and lung tissue. The preprocessing stage suppresses the very dark background pixels, improves the nodules' visibility, and facilitates the subsequent image processing stage. Morphological operations and thresholding were performed to obtain the lung mask. Wavelet-based denoising suppresses the noise. Binary segmentation using Otsu thresholding and morphological operations was used to refine the parenchyma mask. The enhanced image and parenchyma mask are intersected to obtain the lung parenchyma in the region extraction stage. Wavelet-based quantification enhances the structural and texture information of lung parenchyma. The Canny edge detector defines the boundaries of the nodule and parenchyma. A manual interpretation is required to select the nodule and parenchyma by clicking on the edges. Horizontal and vertical endpoints need to be selected physically on the edge points to measure the mean diameter. Finally, the segmented nodule and estimated mean diameter are displayed.

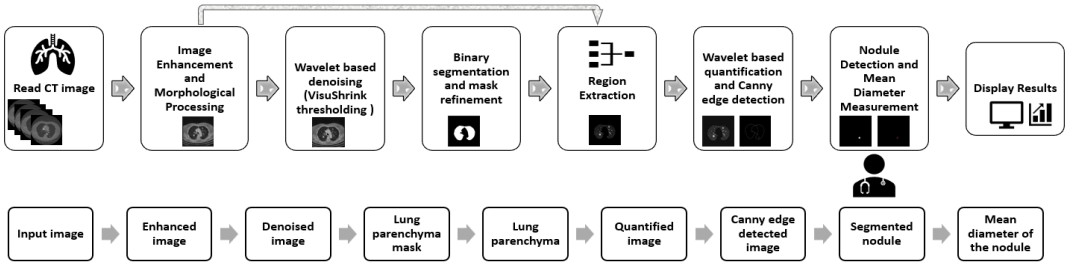

Figure 1. Workflow of lung nodule segmentation and nodule measurement

Let I be the CT image of size 512×512 pixels. The contrast enhance image is given by:

$$I_{CE} = (\frac{I-I_{min}}{I_{max}-I_{min}})^{\gamma} \quad (1)$$

Where I_{min}=0.02, $I_{max} = 60$, gamma correction γ= 2.5.
Morphological operations suppress the artifacts and smoothen the object noundaries:

$$I_{open} = (I \ominus B) \oplus \mathrm{B} \quad (2)$$

B =10 is a structural element, $\ominus = Erosion$, $\oplus = Dilation$

Image is decomposed using haar discrete wavelet transform to obtain approximation and detailed coefficients [13]:

$$I_{DWT} = \{cA, cH, cV, cD\} \quad (3)$$

cA = Approximation co efficients.
cH, cV, cD= detailed coefficients.
Average of median of all the coefficients are given by:

$$M = (\frac{(median(cA)+median(cH)+median(cV)+median(cD))}{4}) \quad (4)$$

The satnderd deviation $\sigma = \frac{M}{0.6745}$ (5)

Visushrink threshold is given by:

$$UT = \sigma\sqrt{2\ln(M)} \quad (6)$$

M is a wavelet co efficients:

$$softThreshold = @(x,t)\ sign(x)\ .*\ max(abs(x) - UT, 0); \quad (7)$$

Soft threshold applied to all the wavelet coefficients then the denoised image is obtained by applying inverse discrete wavelet transform:

$$I_{IDWT(Denoised)} = \{cA_{ST}cH_{ST}cV_{ST}cD_{ST}\} \quad (8)$$

Otsu thresholding separates lung region and non lung regions by maximizing class varience. It is used to obtain the binary mask:

$$I_{Binary} = \begin{Bmatrix} 1,\ I_{IDWT(Denoised)}(x,y) > T \\ 0,\ I_{IDWT(Denoised)}(x,y) < T \end{Bmatrix} \quad (9)$$

Morphological closing operation connects the fragmented region to obtain the lung parenchyma mask:

$$I_{Lung\ parenchyma\ mask} = (I \oplus B) \ominus \mathrm{B} \tag{10}$$

Lung region extracted by overlay of contrast enhanced image and lung parenchyma mask:

$$I_{Lung\ parenchyma} = I_{Lung\ parenchyma\ mask} \times I_{CE} \tag{11}$$

The quantification performed using haar wavelet transform. The image is decomposed into approximation and detailed coefficients the quantized by 2. These coefficients are used to obtain quantified image by applying IDWT. The quantified image preserves the significan nodule features by suppressing small variations and weak details of the image:

$$I_{Quantification} = \left(IDWT(Quantizeby\ 2\left(DWT\left(I_{Quantification}\right)\right)\right) \tag{12}$$

Canny edge detection is applied to the wavelet decomposed coefficients with the threshold value of 0.1 for better edge localization, and to produce thin and continuous edges.

$$I_{Edge} = \begin{Bmatrix} 1, & G > 0.1 \\ 0, & Otherwise \end{Bmatrix} \tag{13}$$

Where G=$\sqrt{G_x^2 + G_y^2}$ gradient magnitude in the direction of $\theta = tan^{-1}(\frac{G_x^2}{G_y^2})$.

The labelled image represents the segmented nodule or segmented parenchyma of the given CT image:

$$I_{segmeted\ image} = I_{labelled} \tag{14}$$

The mean diameter of the nodule is obtained by orthogonal diameters whose end points are selected manually. The real word distance of the selected nodule is given by:

$$Mean\ diameter\ of\ the\ nodule = 0.036 \times \sqrt{a^2 + b^2} \tag{15}$$

a and b are orthogonal line segments obtained from the region of interst by manual intervention. Pulmonary nodules magnitude ratio (PNMR) is defined as the ratio of mean diameter of the pulmonary nodule to the mean diameter of the corresponding lung parenchyma as shown in the Figure 2:

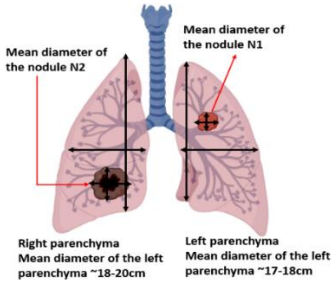

Figure 2. PNMR assessment

$$\text{Pulmonary nodules magnitude ratio (PNMR)} = \frac{Mean\ diameter\ of\ the\ nodule}{Mean\ diameter\ of\ the\ parenchyma} \times 100 \tag{16}$$

2.3. Synthetic nodules construction

Synthetic nodules are generated to evaluate the proposed nodule quantification approach. As shown in Figure 3, the input CT image is subjected to the thresholding and morphological operations to obtain the

largest connected regions that represent the lung parenchyma. The random location is selected manually, and an irregular shape is generated with polar coordinate boundary modulation to mimic the irregular structure of the nodule. the Gaussian intensity core, internal heterogeneity, texture variations, and peripheral boundary variations introduced to match the original pulmonary nodules. The generated synthetic nodules were embedded into the original CT image. The corresponding nodule ground truth was also generated to evaluate the model performance.

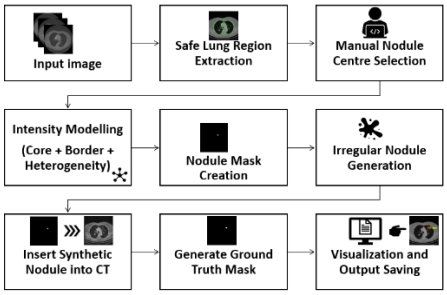

Figure 3. Construction of synthetic nodules

Let P $(x_c y_c)$ be the selected coordinate points that represent the center of the nodule in the lung CT image. The polar coordinate representation of the selected point is given by:

$$R = \sqrt{dx^2 + dy^2} \text{ and } \theta = tan^{-1}(\frac{dx}{dy}) \quad (17)$$

$dx = x - x_c$, $dy = y - y_c$, x and $y\ are$ each pixel coordinates.
The irregular boundary of the nodule is obtained by the nominal radius r and it is repreneted by:

$$R_{Irregular\ boundary} = (\theta) = r[0.18\sin(20\theta) + 0.2\cos\sin(9\theta) + 0.10\sin(9\theta)] \quad (18)$$

The nodule mask is obtained by:

$$I_{NM}(x,y) = \begin{Bmatrix} 1, & R \le R_{boundary} \\ 0, & R > R_{boundary} \end{Bmatrix} \quad (19)$$

The Gaussian core intensity is given by:

$$I_{core}(x,y) = A\ \exp(\frac{-R^2}{2\sigma^2}) \quad (20)$$

A is a core intensity amplitude 0.7<A<0.8, A= 0.7+0.1×rand, $\sigma = nodule\ radius/2.5$. Boundary enhancement of the nodule is given by:

$$I_{boundary} = 0.55\ \exp(\frac{-(R-R_b)^2}{2w^2}) \quad (21)$$

Border width is given by w=0.25r, $R_b = 0.85R_{Irregular\ boundary}$. Internal heterogeneity of the nodule is given by:

$$I_{Hetero} = 0.15.\ G(x,y)\ I_{NM}(x,y) \quad (22)$$

$G(x,y)$ is Gaussian smoothening field. Final synthetic nodule is given by:

$$I_{nodule} = (I_{core} + I_{boundary} + I_{heter}).I_{NM}(x,y) \quad (23)$$

Intensity normalization using min max normalization. It is impremented to obtain standard intensitity values among core, boundary and nodule texture. It scales the nodule intensity range [0,1] and facilitating unified integration into CT image:

$$I_{Nodule\ norm} = \frac{I_{nodule} - I_{min}}{I_{max} - I_{min}} \quad (24)$$

Normalized nodule integrated into original CT image using pixel wise intensity suppression:

$$I_{Synth\ CT} = I_{Nodule\ norm} + I_{CT} \quad (25)$$

Intensity clipping limit the pixel values [0,1] and prevent intensity overflow ofter adding nodule into CT image:

$$I_{Synth\ CT} = \min(I_{Synth\ CT}, 1) \quad (26)$$

A synthetic nodule generated and placed inside the CT image comprises spiculated margins, a dense intensity core, and random texture to mimic the original pulmonary nodule demonstrated in Figure 4. Multiple nodules with different dimensions can be integrated in a single instance.

3. RESULTS AND DISCUSSION

3.1. Assessment of nodule segmentation

The experiments were conducted in a MATLAB environment on an Intel® Core™ i3-1005G1 CPU operating at 1.20 GHz. The lung nodule segmentation performance was evaluated using standard segmentation metrics. The nodule segmentation was performed on the single representative CT image from the LIDC-IDRI dataset and evaluated against the corresponding ground truth image. As shown in Figure 4, our proposed method segments the lung nodule effectively. The input CT image is subjected to segmentation and quantification to extract the significant features of the image as shown in Figure 4(a), and then Canny edge detection is applied to obtain the boundaries of the nodule and lung parenchyma as shown in Figures 4(b) and (c). This stage is more crucial because the nodule boundary itself is a region of interest for measuring the mean diameter of the nodule Figures 4(d) and (e).

The quantitative analysis for nodule segmentation was performed for the proposed method. Simulation results obtained in Table 1 were obtained from a single CT image and its corresponding ground truth from the LIDC-IDRI dataset rather than the large test cohort. It is a preliminary assessment of the proposed model and doesn't establish the clinical robustness. The standard segmentation performance metrics [14] are used to compare performance with other models. The proposed model achieved a Dice coefficient of 0.8852, indicating a strong overlap between the predicted lung nodule and the ground truth. The segmentation accuracy is further evaluated using IOU. An IOU of 0.7941 represents that the proposed model accurately localizes the lung nodule regions and maintains the precise boundary delineation. The class imbalance of the background pixels dominates the specificity, precision, and accuracy of all the models. 0.8096 of sensitivity and 0.9765 of precision represent the correctly identified nodule pixel. The proposed model achieved low sensitivity and high precision, indicating that the model accurately detects the prominent lung nodules without false positives, which is the most prominent characteristic in the medical image analysis. A 0.8852 F1 score represents the most reliable segmentation performance. The proposed segmentation framework outperforms the Gaussian mixture model, fuzzy C-means, and K-means [15]-[18]. Overall, the proposed model confirms the reliability, robustness, and accuracy of the nodule segmentation framework for automatic pulmonary nodule localization and segmentation.

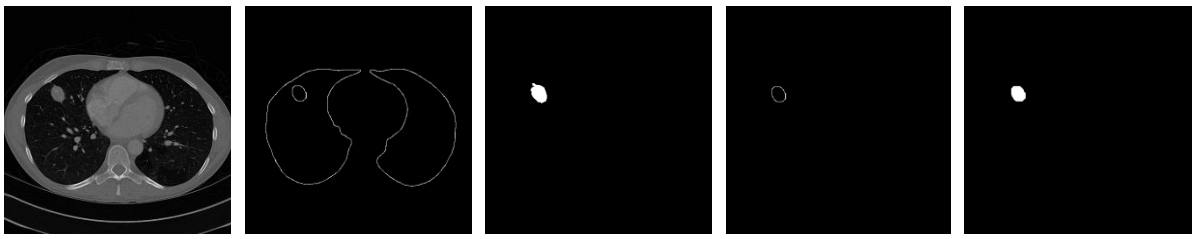

(a) (b) (c) (d) €

Figure 4. Pulmonary nodule segmentation from the CT image: (a) original CT image, (b) canny edge detected image, (c) nodule ground truth, (d) nodule boundary, and (e) segmented nodule

Table 1. Nodule segmentation performance

Metric	Proposed method	Gaussian Mixture Model	Fuzzy C- Means	K- Means
Dice Similarity	0.8852	0.8704	0.8577	0.5628
IOU	0.7941	0.7705	0.7509	0.3916
Sensitivity	0.8096	0.7733	0.7529	0.8770
Specificity	0.9999	1.0000	1.0000	0.9970
Accuracy	0.9991	0.9990	0.9989	0.9967
Precision	0.9765	0.9954	0.9965	0.4143
F1 Score	0.8852	0.8704	0.8577	0.5628

3.2. Assessment of pulmonaryg nodule magnitude

The pulmonary nodules of variable size and structures are generated to evaluate the proposed pulmonary nodule magnitude ratio (PNMR) as shown in Figure 5. Sample 1 consists of a nodule diameter of 22 mm with 48% irregularity, 80% normalized intensity with a Gaussian decay profile, an irregular border with a peak intensity of 0.55, and a speculation ranging from 0.5 to 0.55 to mimic the original pulmonary nodule. This synthetic nodule is implanted in the left side of the lung parenchyma as shown in Figure 5(a). Sample 2 was generated with a nodule diameter of 15 mm on the right side of the lung parenchyma as shown in Figure 5(b). Sample 3 and sample 4 extend the size of the nodule from 25 mm to 33 mm as shown in Figures 5(c) and (d).

Synthetic nodules generated of different sizes and spiculations are then integrated into a single CT image as shown in Figure 6. The nodules are extracted by segmentation, quantification, and Canny edge detection applied to the CT image. Figure 6(a) segmentation extracts the region of interest, and quantification is used to obtain the meaningful numerical measurements [19]. Figure 6(b) represents the Canny edge-detected image capable of identifying the boundaries of parenchyma, original nodule, and synthetic nodule. The region of interest needs to be selected manually; the endpoints of the vertical and horizontal diameter lines need to be selected manually. The mean diameter obtained by the average of the orthogonal lines selected before. This procedure was repeated for nodules and the lung parenchyma, correspondingly, to obtain the pulmonary nodules' magnitude ratio. Figures 6(c) and (d) represents the lung parenchyma and nodule quantities used in PNMR.

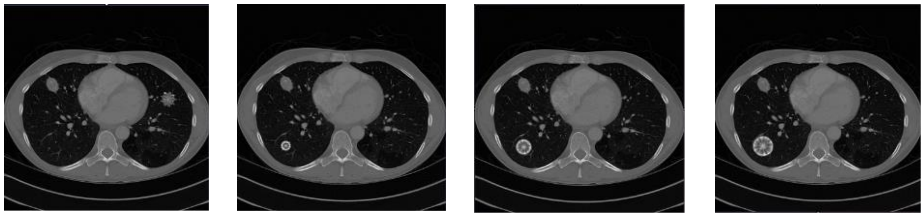

(a) (b) (c) (d)

Figure 5. Synthetic pulmonary nodule generation with variable size: (a) Sample-1(22mm), (b) Sample-2 (15mm), (c) Sample-3 (25mm), and (d) Sample-3 (33mm)

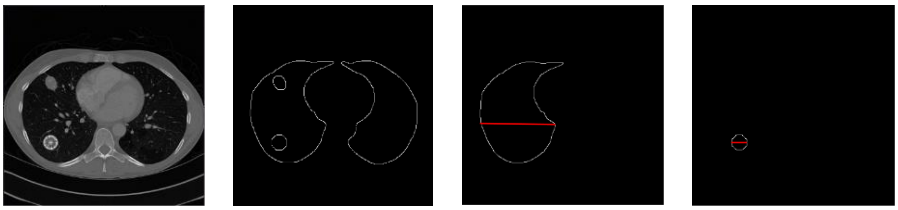

(a) (b) (c) (d)

Figure 6. PNMR quantities: (a) CT image with synthetic nodule, (b) cannty edge detected image, (c) lung parenchyma measurement, and (d) nodule measuerement

Table 2 demonstrates the pulmonary nodule magnitude ratio (PNMR) of all the synthetic nodules. Sample-1 exhibits little deviation in the nodule measurement with 9.7% relative error due to its spiculated structure. Sample -2 of 1.6%, Sample -3 of 0.34%, and Sample 4 of 0.56% have respective relative errors. The circular nodules exhibit less relative error than the spiculated nodules. Sample 2-Sample 4 nodule PNMR

increases with the increasing nodule dimension; it is a key factor that can be used to evaluate the growth rate of pulmonary nodules.

Table 2. PNMR

Samples	Actual Nodule size (mm)	Measured Nodule size (mm)	Absolute error	Parenchyma size (mm)	PNMR (%)
Sample-1	22	19.974	2.136	132.221	15.1
Sample-2	15	14.248	0.248	143.185	9.9
Sample-3	25	25.096	0.096	143.185	17.5
Sample-4	33	32.186	0.186	143.185	22.47

3.3. Comparision with the existing method

The proposed nodule segmentation results compared with the existing methods tabulated in the Table 3. Models such as transformers, UNet, encoder-decoder based models and deep learneing architectures performed excell, achived Dice score above 0.8. these models learn the hierarchical features of the image and preserve spatial details make them to detect the nodules effectively. Although the deep learning methods demonstrated superior performance, our traditional method yields the competitive results under favarable conditions.

Table 3. Comparartive study of prevailing methods

Method	Metrics
Hybrid transformer UNet [20]	DSC=93.00%, IOU=86.00%, Precision =90.00%, Recall= 95.00% for client 2
Lung-Mamba [21]	DSC=96.48%
IGSM-Enhanced encoder-decoder network [22]	mIOU= 0.7735, Dice= 0.9665, accuracy= 0. 9873
Daisy-Net [23]	IOU= 81.41%, Dice= 89.75%, Precision = 95.34%, Sensitivity = 84.78%, Specificity =99.994
Few-Shot Joint Segmentation and Classification [24]	Mean IOU=69.36%
squeeze excitation dilated attention based residual UNet [25]	DSC=97.86%, IOU=96.4%, Sensitivity =96.54%, Precision =98.84%
Proposed method	DSC=0.8852, IOU =0.7941, Sensitivity=0.8096, Specificity=0.9999, Accuracy =0.9991, Precision = 0.9765, F1 Score= 0.8852

3.4. Limitations and future scope

The simulation work is conducted on the LIDC-IDRI CT image; synthetic nodules of different sizes and structures are created to test the algorithm robustness and validate the proposed method under different conditions. It requires rigorous validation across diverse real-time clinical datasets to confirm the clinical deployment. The future work will focus on diverse datasets and real-time data, including continuous monitoring of nodule growth and related ailments, to enhance the generalizability of the pulmonary nodule magnitude ratio.

4. CONCLUSION

In this work, effective pulmonary nodule segmentation and nodule assessment using the pulmonary nodule magnitude ratio method were proposed. Our proposed model can effectively segment the pulmonary nodules automatically and define their boundaries for semiautomatic nodule assessment. A novel pulmonary nodule magnitude ratio was tested on synthetic nodules in the CT image, which defines the nodule growth rate. The proposed segmentation method achieved a Dice of 88.52%, surpassing the other traditional methods. The proposed method consistently produces enhanced results across multiple evaluation stages. The competitive performance with the deep learning-based models suggests the effectiveness of pulmonary nodule segmentation in limited computational resources and datasets.

ACKNOWLEDGMENTS

I am conducting this work as part of my Ph.D. research at the Department of Electronics and Communication, Sri Siddhartha Institute of Technology. Sri Siddhartha Academy of Higher Education, Karnataka, India.

FUNDING INFORMATION

This research received no specific grant from any funding agency in the public, commercial or not for profit sectors.

AUTHOR CONTRIBUTIONS STATEMENT

This journal uses the Contributor Roles Taxonomy (CRediT) to recognize individual author contributions, reduce authorship disputes, and facilitate collaboration.

Name of Author	C	M	So	Va	Fo	I	R	D	O	E	Vi	Su	P	Fu
Asharani Ramadas	✓	✓	✓	✓	✓	✓	✓	✓	✓	✓	✓			
Chidananda Murthy Melekote Vinayakamurthy		✓				✓				✓		✓	✓	

C : **C**onceptualization
M : **M**ethodology
So : **So**ftware
Va : **Va**lidation
Fo : **Fo**rmal analysis
I : **I**nvestigation
R : **R**esources
D : **D**ata Curation
O : Writing - **O**riginal Draft
E : Writing - Review & **E**diting
Vi : **Vi**sualization
Su : **Su**pervision
P : **P**roject administration
Fu : **Fu**nding acquisition

CONFLICT OF INTEREST STATEMENT

The authors state they have no rival interests.

INFORMED CONSENT

The data set used in this work is publicly available database consisting of anonymized medical images provided for research pupose, hence No consent is required for the secondary analysis.

ETHICAL APPROVAL

The data set utilized in this study is publicly accessible and created for research purposes; hence, no ethical approval was taken.

DATA AVAILABILITY

Data availability does not apply to this paper because this study did not create any new data.

REFERENCES

[1] M. L. Mullin *et al.*, "Upstaging of screen-detected lung cancers during diagnostic assessment," *Thorax*, p. thorax–2025–224006, Feb. 2026, doi: 10.1136/thorax-2025-224006.
[2] A. Snoeckx *et al.*, "Lung cancer screening with low-dose CT: definition of positive, indeterminate, and negative screen results. A nodule management recommendation from the European Society of Thoracic Imaging," *European Radiology*, vol. 36, no. 1, pp. 135–147, 2025, doi: 10.1007/s00330-025-11648-4.
[3] M. Prokop *et al.*, "Aggressiveness-guided nodule management for lung cancer screening in Europe—justification for follow-up intervals and definition of growth," *European Radiology*, vol. 36, no. 1, pp. 122–134, 2025, doi: 10.1007/s00330-025-11647-5.
[4] M.-P. Revel *et al.*, "ESR Essentials: lung cancer screening with low-dose CT—practice recommendations by the European Society of Thoracic Imaging," *European Radiology*, vol. 36, no. 3, pp. 2064–2073, Aug. 2025, doi: 10.1007/s00330-025-11910-9.
[5] W. Liu, Y. Wu, W. Yu, M. J. Bittle, Z. Zheng, and H. Kharrazi, "Measuring the impact of AI on report-drafting efficiency in chest computed tomography interpretation: retrospective analysis," *Journal of Medical Internet Research*, vol. 28, p. e77967, Mar. 2026, doi: 10.2196/77967.
[6] J. Geppert *et al.*, "Software with artificial intelligence-derived algorithms for detecting and analysing lung nodules in CT scans: systematic review and economic evaluation," *Health Technology Assessment*, pp. 1–234, May 2025, doi: 10.3310/jytw8921.
[7] Y. Mao *et al.*, "Assessments of lung nodules by an artificial intelligence chatbot using longitudinal CT images," *Cell Reports Medicine*, vol. 6, no. 3, p. 101988, Mar. 2025, doi: 10.1016/j.xcrm.2025.101988.
[8] C. McCabe, E. Abadi, M. Zarei, W. P. Segars, and E. Samei, "The potential of photon-counting CT for the improved precision of lung nodule radiomics," *Physics in Medicine & Biology*, vol. 70, no. 3, p. 35001, Jan. 2025, doi: 10.1088/1361-6560/adaad2.
[9] J. Paramasamy *et al.*, "Validation of a commercially available CAD-system for lung nodule detection and characterization using CT-scans," *European Radiology*, vol. 35, no. 2, pp. 1076–1088, 2024, doi: 10.1007/s00330-024-10969-0.
[10] S. Chen, L. Gao, M. Tan, K. Zhang, and F. Lv, "Performance evaluation of four deep learning-based CAD systems and manual reading for pulmonary nodules detection, volume measurement, and Lung-RADS classification under varying radiation doses and reconstruction methods," *Diagnostics*, vol. 15, no. 13, p. 1623, 2025, doi: 10.3390/diagnostics15131623.
[11] M. M. Hammer, "Comparison of volume-based and diameter-based assessment of solid nodules in lung cancer screening," *Thorax*, vol. 80, no. 9, pp. 579–579, 2025, doi: 10.1136/thorax-2025-223295.

[12] "Checking your browser - reCAPTCHA." https://www.kaggle.com/datasets/jokerak/lidcidri (accessed Jun. 11, 2026).
[13] R. K. Paul, S. Jena, S. Chandran, A. Bandyopadhyay, and S. Swain, "Image compression scheme based on optimized K-means clustering and higher-level decomposed DWT," *Procedia Computer Science*, vol. 235, pp. 642–655, 2024, doi: 10.1016/j.procs.2024.04.063.
[14] D. Müller, I. Soto-Rey, and F. Kramer, "Towards a guideline for evaluation metrics in medical image segmentation," *BMC Research Notes*, vol. 15, no. 1, Jun. 2022, doi: 10.1186/s13104-022-06096-y.
[15] Y. Yu *et al.*, "Techniques and challenges of image segmentation: a review," *Electronics*, vol. 12, no. 5, p. 1199, Mar. 2023, doi: 10.3390/electronics12051199.
[16] D. Krasnov, D. Davis, K. Malott, Y. Chen, X. Shi, and A. Wong, "Fuzzy C-means clustering: a review of applications in breast cancer detection," *Entropy*, vol. 25, no. 7, p. 1021, 2023, doi: 10.3390/e25071021.
[17] H. Mittal, A. C. Pandey, M. Saraswat, S. Kumar, R. Pal, and G. Modwel, "A comprehensive survey of image segmentation: clustering methods, performance parameters, and benchmark datasets," *Multimedia Tools and Applications*, vol. 81, no. 24, pp. 35001–35026, Feb. 2021, doi: 10.1007/s11042-021-10594-9.
[18] X. Liu, Y. Zhao, S. Wang, and J. Wei, "G-SAM: GMM-based segment anything model for medical image classification and segmentation," *Cluster Computing*, vol. 27, no. 10, pp. 14231–14245, 2024, doi: 10.1007/s10586-024-04679-x.
[19] R. Asharani and M. V Chidananda Murthy, "Image segmentation and quantification using wavelet transform," in *Artificial Intelligence and Technology: Systems Management, Decisions and Control for Sustainability in the Digital Age*, Springer Nature Switzerland, 2026, pp. 553–565.
[20] S. M. Turjya and M. Fawakherji, "Federated lung nodule segmentation using a hybrid transformer–U-Net architecture," *Scientific Reports*, vol. 16, no. 1, Jan. 2026, doi: 10.1038/s41598-026-35243-9.
[21] H. T. Gayap and M. A. Akhloufi, "Lung-Mamba: Lung nodule segmentation model optimized by Mamba's selective state spaces," *Biomedical Engineering Advances*, vol. 11, p. 100214, 2026, doi: 10.1016/j.bea.2026.100214.
[22] M. A. Thanoon *et al.*, "A symmetric encoder–decoder network with enhanced group–shuffle modules for robust lung nodule detection in CT scans," *Biomimetics*, vol. 11, no. 2, p. 92, Feb. 2026, doi: 10.3390/biomimetics11020092.
[23] Z. Zhu *et al.*, "Daisy-Net: dual-attention and inter-scale-aware yield network for lung nodule object detection," *Mathematics*, vol. 14, no. 8, p. 1350, Apr. 2026, doi: 10.3390/math14081350.
[24] M. A. Rahim, M. Awais, and M. Mahmud, "Few-shot joint segmentation and classification of lung nodules in CT with self-supervised correlation transformers," *Proceedings of the IEEE/CVF Conference on Computer Vision and Pattern Recognition*, pp. 6328–6337, 2026.
[25] D. Alhajim, K. Ansari-Asl, G. Akbarizadeh, and M. N. Soorki, "Improved lung nodule segmentation with a squeeze excitation dilated attention based residual UNet," *Scientific Reports*, vol. 15, no. 1, Jan. 2025, doi: 10.1038/s41598-025-85199-5.

BIOGRAPHIES OF AUTHORS

Asharani Ramadas is a research Scholar at Sri Siddhartha Academy of Higher Education, Tumkur, Karnataka, India. She is graduated in Telecommunication Engineering and master of Technology in Digital Electronics and Communication Engineering from Vishweshwaraiah Technological University, Karnataka, India. She is an assistant professor at Ramaiah College of Arts Science and Commerce, Bengaluru, India. Her research includes the medical image processing, artificial intelligence and machine learning. She can be contacted at email: asha.srp@gmail.com.

Chidananda Murthy Melekote Vinayakamurthy is an Associate professor at Sri Siddhartha Academy of Higher Education in the Department of Electronics and Communication. He received his B.E., M.Tech., and Ph.D. from Visvesvaraya Technological University in 2005, 2007, and 2019, respectively. In addition to giving presentations at conferences, he has 26 papers published in journals. His areas of interest in study are computer vision, machine learning, and high-resolution images. He can be contacted at email: chidanandamurthymv@ssit.edu.in.